Double-Directional Channel Measurements for Urban THz Microcellular Communications in a Street Canyon

Naveed A. Abbasi*, Jorge Gomez-Ponce*†, Revanth Kondaveti*, Ashish Kumar*, Eshan Bhagat*,
Rakesh N. S. Rao*, Shadi Abu-Surra‡, Gary Xu‡, Charlie Zhang‡, Andreas F. Molisch*
*University of Southern California, Los Angeles, CA, USA
†ESPOL Polytechnic University, Guayaquil, Ecuador
‡Samsung Research America, Richardson, TX, USA
Email: {nabbasi, gomezpon, kondavet, akumar63, ebhagat, nayaksom, molisch}@usc.edu,
{shadi.as, gary.xu, jianzhong.z}@samsung.com

***Abstract*—THz communication has attracted a great deal of attention due to the large bandwidth available in this band. However, system development and deployment requires detailed knowledge of the wireless channel, which must be provided by measurements (channel sounding) and subsequent modeling in key scenarios of interest. One important scenario in this regard is the urban outdoor microcellular scenario where the Transmitter (Tx) and the Receiver (Rx) have a significant height difference. In this paper, we present ultra-wideband double-directional channel measurements in a microcellular scenario for the band between 145-146 GHz in a street canyon with Tx-Rx of distances up to 67 m. The results are analyzed in the delay and angular domain, and the impact of the street canyon on the power delay profiles and angular power spectra is detailed. These measurements thus contribute towards the creation of a more realistic and detailed THz channel model in these scenarios.**

***Index Terms*—Terahertz (THz) communication, urban scenario, double-directional channel measurements, microcellular scenario**

I. Introduction

The tremendous data rates required for new and upcoming applications such as virtual reality and immersive environment are beyond the capabilities of current mmwave-based 5G communication systems [1], [2]. To fulfill these new demands, it is necessary to explore new higher frequencies such as the THz band,[1] which is mostly unused at the moment. Keeping this in mind, the Federal Communications Commission (FCC) recently offered experimental licenses in the lower THz band so that a better understanding of these bands can be developed.

In order to design a communication system for a particular frequency band of interest, it is imperative to understand the characteristics of the wireless channel the system will operate in. Thus, we need to perform channel sounding measurements that allow to analyze the channel and provide key channel parameters that can be utilized in the design of a communication system [3]. Since 6G systems in the THz range will use adaptive directional antennas, double-directional channel measurements (i.e., directionally resolved at both transmitter (Tx) and receiver (Rx)) are required.

A number of double-directional propagation studies have been conducted in the THz band (0.1-10 THz), especially in the segment between 0.1-0.5 THz. Most of these studies are focused on short-distance cases that are generally indoors e.g., [4], [5], typically due to inherent limitations of the measurement setups. However, outdoor deployments typically target wider coverage: in scenarios such as microcellular cases where the base station (BS) is elevated relative to the user equipment (UE), cell radii of 100 m or more are envisioned. Several recent studies have overcome the above-mentioned limits of typical THz channel sounding setups, and performed double-directional measurements over longer distances and in outdoor scenarios. The first long-distance (100 m) double-directional channel measurements were for the 140 GHz band, reported in [6] in 2019 by our group, as well as our more works [7], [8] where we target the device-to-device (D2D) scenario. Moreover, recently [9], [10] reported channel measurements and path loss modeling at 140 GHz over longer distances in an urban scenario, with the BS elevated 4 m above the ground, which is similar to the heights of lamp posts.

The current paper aims to analyze a microcell scenario where the Tx is significantly higher, namely at 11.5 m, which is comparable to a typical microcell BS height. More specifically, we present results for microcellular urban outdoor scenarios based on ultra-wideband double-directional channel measurements between 145-146 GHz, conducted at 7 different transmitter (Tx) - receiver (Rx) location pairs in a street canyon. Four of these points are non-line-of-sight (NLoS) and three locations are line-of-sight (LoS). We analyze power delay profiles, delay spread, multipath component (MPC) power distribution, angular power spectra and angular spread. To the best of our knowledge, such a channel measurement campaign for the current scenario has not been reported before. Results from more measurement locations, including a statistical analysis, will be provided in an extended journal version [11].

[1] The frequency band discussed in this paper, namely 140 GHz, has been called variously "high mmWave", "sub-THz", and "THz". For conciseness and in keeping with popular notation in the communications literature, we use the term THz henceforth.

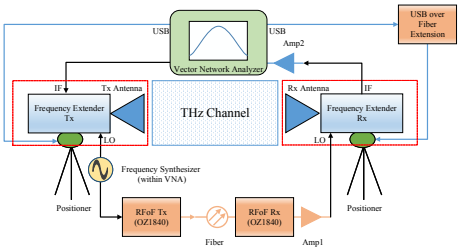

Fig. 1: Channel sounding setup.

Fig. 2: Site map.

The organization of this paper is as follows: In section II we describe the measurement setup and site. In Section III, we highlight our key results. Finally, we conclude the manuscript in Section IV.

II. Measurement Equipment and Site

A. Testbed description

Our measurement campaign is carried out by using a frequency-domain channel sounder (see Fig 1). The main component of this equipment is the vector network analyzer (VNA) which allows scans in a designated frequency range. Due to limitations in the VNA's frequency range, we use frequency extenders to help us reach the THz domain. Other limitations are range and the high attenuation levels of RF cables in THz bands that compromise the maximum measurable distance of the system (usually < 10m). For this reason, an RF-over-fiber (RFoF) connection between the VNA and the frequency extenders in the Tx and Rx is used, allowing us to perform long-distance measures ($\approx$ 100 m). Further explanations about the design and principles behind the RFoF system are described in [12]. To eliminate the effects of the "system and antennas" from the measurement, we perform a time-gated over-the-air (OTA) calibration every day of the measurement campaign.

Mechanical positioners rotate the antennas into various directions, providing a scan in both azimuth and elevation to provide double-directional channel characteristics of the channel. Due to the characteristics of the VNA and the mechanically rotating antennas, each measurement lasted several hours, therefore, the measurement were performed at night to ensure that no significant moving objects were present during the experiment.

B. System settings

The settings and variable names for the VNA, frequency extenders, and mechanical positioners (rotors) are described in Table I. Each frequency sweeps scans a 1 GHz bandwidth with a resolution of 1MHz. In other words, 1001 points are obtained per scan. Consequently, the maximum measurable excess delay is 1μs or 300 m of maximum measurable distance, which is enough to cover all significant multipath components.

Given that we are interested in microcellular scenarios, Tx and Rx were set at different heights. Following the 3GPP recommendation [13] we placed the Tx at 11.5m from the ground and the Rx at 1.7m. The positioners (rotors) for this experiment were set to align the Tx and Rx such that the azimuth angle, $\phi = 0°$ and the elevation angle $\tilde{\theta} = 0°$ will correspond to the LoS for all points in the campaign. Both Tx and Rx scans are performed over 3 elevations separated 13° ($\tilde{\theta}_{Tx}, \tilde{\theta}_{Rx} \in \{-13°, 0°, 13°\}$). The azimuthal scan in the Tx is taken over the range of $-60°$ to $60°$ in $10°$ steps, corresponding to a typical BS microcell sector antenna. At the Rx, a complete scan from $0°$ to $360°$, with the same granularity as the Tx side, is performed. [2]

C. Site description

The measurements are performed in a street canyon of approximately 6 meters width located between Technical Theatre Laboratory (TTL) and Scene Dock Theatre (SCD) buildings and in front of the Downey Way Parking Structure (PSA) at the University of Southern California, University Park Campus in Los Angeles, California, USA. A map with the detailed scenario description is shown in Fig. 2. This area has walls, parked cars on one side, and foliage at the street canyon entrance and in front of PSA.

TABLE I: Setup parameters.

Parameter	Symbol	Value
Measurement points	N	1001
Tx height	h_{Tx}	11.5 m
Rx height	h_{Rx}	1.7 m
IF bandwidth	IF_{BW}	10 KHz
Antenna 3 dB beamwidth	$\tilde{\theta}_{3dB}$	13°
Tx Az rotation range	ϕ_{Tx}	[-60°,60°]
Tx Az rotation resolution	$\Delta\phi_{Tx}$	10°
Rx Az rotation range	ϕ_{Rx}	[0°,360°]
Rx Az rotation resolution	$\Delta\phi_{Rx}$	10°
Tx El rotation range	$\tilde{\theta}_{Tx}$	[-13°,13°]
Tx El rotation resolution	$\Delta\tilde{\theta}_{Tx}$	13°
Rx El rotation range	$\tilde{\theta}_{Rx}$	[-13°,13°]
Rx El rotation resolution	$\Delta\tilde{\theta}_{Rx}$	13°

TABLE II: Description of Tx-Rx links and their respective direct distances.

Tx identifier	Rx identifier	$\mathbf{d_{Tx-Rx}}$ (m)
Tx_1 (LoS)	1-3	36.3, 57.9, 65.7
Tx_2 (NLoS)	4-7	35, 45.5, 58.5, 66.8

The Tx is set in the third floor of Downey Way Parking Structure (PSA), facing west towards the street canyon to emu-

[2] $\tilde{\theta} = 0°$ is not equivalent to $\theta = 90°$ in elevation

late a microcellular scenario. The Rx was placed on the paved ground in two Routes, one for LoS and another for NLoS. Route 1 consists of 3 points located in the middle of the street canyon facing east towards the Tx. The distances between the Tx and the Rx locations are between approximately 36 and 65 meters. Route 2 consists of 4 Rx locations situated in the same street canyon as Route 1 points. Tx was 15 meters south of the Tx location for the previous route; doing so blocked the LoS with the TTL building. A detailed description of the distances between Tx and Rx for all points is given in Table II.

III. Processing of measurements

The VNA based measurement setup explained in Section II produces a collection of frequency scans for each Tx-Rx geographical location. Each measurement can be described as a five-dimensional tensor $H_{meas}(f, \phi_{Tx}, \tilde{\theta}_{Tx}, \phi_{Rx}, \tilde{\theta}_{Rx}; d)$ where f represents the frequency points over the 1 GHz bandwidth (145-146 GHz), ϕ_{Tx} and ϕ_{Rx} represent azimuth orientation of the Tx and Rx, $\tilde{\theta}_{Tx}$ and $\tilde{\theta}_{Rx}$ represent elevation orientation of the Tx and Rx, and d is the Tx-Rx distance. Each tensor H_{meas} has dimensions $N \times N^{\tilde{\theta}}_{Tx} \times N^{\phi}_{Tx} \times N^{\tilde{\theta}}_{Rx} \times N^{\phi}_{Rx}$ where N is the number of frequency points per sweep (1001), $N^{\tilde{\theta}}_{Tx}$ and $N^{\tilde{\theta}}_{Rx}$ are the number of azimuth directions at the Tx (13) and Rx (36), and N^{ϕ}_{Tx} and N^{ϕ}_{Rx} are the number of elevation directions at the Tx and Rx (3) for both.

We eliminate the effect of the system and antennas by performing an OTA calibration which gives us the new "calibrated" channel frequency response (CFR) $H(f, \phi_{Tx}, \tilde{\theta}_{Tx}, \phi_{Rx}, \tilde{\theta}_{Rx}; d)$. Using these calibrated CFRs we proceed to compute multiple parameters, such as the directional power delay profile (PDP):

$$P_{calc}(\tau, \phi_{Tx}, \tilde{\theta}_{Tx}, \phi_{Rx}, \tilde{\theta}_{Rx}; d) = |\mathcal{F}_f^{-1}\{H(f, \phi_{Tx}, \tilde{\theta}_{Tx}, \phi_{Rx}, \tilde{\theta}_{Rx}; d)\}|^2 \quad (1)$$

where $\mathcal{F}_f^{-1}$ is the inverse fast Fourier transform (IFFT) with respect to f. We perform noise and delay thresholding to minimize the cumulative effects of noise and wrap-around in the PDP, similar to [14], by applying a circular shift on the PDP to correct delay bins with power showing up before the LoS:

$$P(\tau) = [P_{calc}(\tau) : (\tau \leq \tau_{gate}) \wedge (P_{calc}(\tau) \geq P_\lambda)] \quad (2)$$

i.e. if $P(\tau)$ does not fulfill the conditions it is considered 0. In this experiment, τ_{gate} is set to have 950 ns of excess delay window from $\tau_{Tx-Rx} = d_{Tx-Rx}/3e8$ (see Table II), where d_{Tx-Rx} is the distance between the Tx and Rx and P_λ is selected to be 15 dB above the noise floor (average noise power) of the PDP.

This analysis will focus on two types of PDPs: the "max-dir" and the omnidirectional . The first is obtained by selecting the antenna direction with the highest power:

$$P_{\max}(\tau) = P(\tau, \phi_{\hat{i}}, \tilde{\theta}_{\hat{j}}, \phi_{\hat{k}}, \tilde{\theta}_{\hat{l}}, d); (\hat{i}, \hat{j}, \hat{k}, \hat{l}) = \max_{i,j,k,l} \textstyle\sum_\tau P(\tau, \phi_i, \tilde{\theta}_j, \phi_k, \tilde{\theta}_l, d) \quad (3)$$

In the second case, we synthesized the omnidirectional PDP by the approach of [15], i.e., selecting the strongest azimuth direction per delay bin to reconstruct the PDP:

$$P^{i,j}_{\text{omni}}(\tau; d) = \max_{\phi_{Tx}, \phi_{Rx}} P(\tau, \phi_{Tx}, \tilde{\theta}^i_{Tx}, \phi_{Rx}, \tilde{\theta}^j_{Rx}; d). \quad (4)$$

where $i, j \in \{1, 2, 3\}$ represents the elevations $(\tilde{\theta}^i_{Tx}, \tilde{\theta}^j_{Rx} \in \{-13°, 0°, 13°\})$ for Tx and Rx respectively. It is important to mention that the previous formula only considers a *single* elevation. To combine all of the elevations we add them up, due to the fact that each elevation capture was done at angles equal to $13°$ (HPBW):

$$P_{\text{omni}}(\tau; d) = \sum_i \sum_j P^{i,j}_{\text{omni}}(\tau; d). \quad (5)$$

Due to the non-ideal antenna pattern, an extra gain is generated from the addition of the different elevations (0.95dB on each end). This "extra" gain is compensated prior the analysis. The procedure to compute the parameters is shown as follows:

1) We obtain the delay spread by computing the second central moment of the PDP [3].
2) We obtain the distribution of power in delay bins. For this, we detect the peaks in the PDPs and sort them to analyze the percentage of power contained in K (with $K = 1, 2, .., N_K$ bins.

$$\gamma(K) = \frac{\sum_{j=1}^{K} P_i(\tau_j)}{\sum_{j=1}^{N_K} P_i(\tau_j)}, \quad (6)$$

where i can be omni-directional or the direction of the strongest power (Max-Dir). The numerator represents the power of the K strongest MPCs and the denominator is the total power of the peaks in the PDP, with N_K the total number of peaks in the PDP. Please note that in the Fourier analysis it is not possible to differentiate between closely spaced MPCs, so the local maximum of the PDP is not strictly identical to an MPC.
3) The path loss (PL) is computed as follows:

$$PL_i(d) = \sum_\tau P_i(\tau, d), \quad (7)$$

where d is the distance between Tx and Rx.
4) Moving to an angular domain analysis, we compute a double-directional angular power spectrum, which is a function of the power concentration over different directions (azimuth, elevation) at Tx and Rx [3]. However, due to an insufficient number of elevation cuts, elevation analysis is not possible, therefore, the angular analysis is solely carried out in azimuth. For this reason, we combine the different elevations by adding them in both link ends.

$$DDAPS(\phi_{Tx}, \phi_{Rx}; d) = \textstyle\sum_{\tilde{\theta}_{Tx}} \sum_{\tilde{\theta}_{Rx}} \sum_\tau P(\tau, \phi_{Tx}, \tilde{\theta}_{Tx}, \phi_{Rx}, \tilde{\theta}_{Rx}; d) \quad (8)$$

this combination is possible because each elevation scan was performed in steps of one HPBW. Using the $DDAPS$ the azimuthal angular power spectrum (APS)

is obtained by integrating over ϕ_{Rx}, and similarly for the APS at the Rx. With the APS, the angular spread is computed by applying Fleury's definition [3] [16]

IV. Measurement results

A. Power delay profiles

As explained in Section II, we observed that the scenario is a "street canyon," therefore, we expected multiple reflections on the sidewalls to impact both PDP and APS. The omni-directional PDPs for all the elevations and various distances are shown in Fig. 3. We make the following key observations:

- The first 2 points (Rx4 and Rx5) show a PDP that is dominated by a single strong reflection, with other MPCs having significantly power, in each case. This effect is shown in all 3 elevations at the receiver.
- Rx6 and Rx7 showed a significant attenuation in the strongest MPC of about 15 dB compared to the previous case. The PDP follows an exponential decay with a rate of 3.76 dB/m for Rx6 and 3.47 dB/m when $\tilde{\phi}_{Rx} = 0$ (it is lower for the other 2 elevations).
- Subsequent MPCs have a larger impact in Rx6 and Rx7 because of the attenuation in the strongest MPC.

Additional insight is possible by analyzing the DDAPS. Received powers are evaluated at discrete directions (the orientations of the horns during the measurements), but for Figs. 4 and 5 we interpolated to improve the resolution of the plots. Points in which the receive power fell below a threshold are shown in white color.

1) RMS delay spread: Rms delay spread σ_τ varies significantly with direction. [4]. It shows low values in directions in which a single MPC, either an LoS, or a strong reflection, dominates. This is observed in Fig. 4 where σ_τ shows values between -90 and -85 dBs concentrated in the range $\theta_{Rx} \in [-60, 60]$ for the entire range of θ_{Tx}. Additionally, we observed σ_τ close to -70 dBs, an effect produced by the fact that no path carries strong power, and the weak paths may stem from reflections by far-away objects. For the NLoS case, Fig. 5 shows a small area where σ_τ takes on values similar to the LoS situations (≈ -85 dBs). These low values are produced due to a dominant reflection in the PDP. σ_τ increases for the rest of the directions (-80 $dBs \leq \sigma_\tau \leq -70$ dBs), due to the multiple reflections and attenuation of the MPCs. Table III shows the values for σ_τ for the "full" omnidirectional case (as described in Eq. 5) and the Max-Dir case. For the LoS points (Route 1), we observe a 3 dBs maximum difference between them; this is relatively small because the LoS component dominates the behavior in either case. For the NLoS case, the difference is much larger, reaching up to 15dBs. An exceptional case is $Tx2-Rx5$ where the difference is ≈ 5 dBs. This fact is related to the high concentration of power in the strongest MPC compared to the rest of the MPCs.

[3] The obtained values are an upper bound for the real angular spread of the channel due to the spread caused by the horn antenna pattern [3]

[4] The results are given on a dBs scale (as is common, e.g., in standardized channel models); the spread on a linear scale is $10^{x/10}$, i.e. -60 dBs corresponds to 1 μs.

TABLE III: σ_τ per location.

$\sigma_\tau(dBs)$	**Omni**	**Max − Dir**
$\mathbf{Tx_1 - Rx_1}$	-81.76	-84.2
$\mathbf{Tx_1 - Rx_2}$	-83.67	-85.59
$\mathbf{Tx_1 - Rx_3}$	-83.4	-84.32
$\mathbf{Tx_2 - Rx_4}$	-82	-91.22
$\mathbf{Tx_2 - Rx_5}$	-85.23	-90.18
$\mathbf{Tx_2 - Rx_6}$	-76.46	-90.12
$\mathbf{Tx_2 - Rx_7}$	-75	-83.24

2) Power distribution over MPCs and path loss: We next analyze the power distribution of the PDP peaks. We compare the results using the "full" Omnidirectional and the Max-Dir PDPs in both cases using the expression in Eq. 6. Fig. 6 shows the distribution for the LoS cases. We observe a high concentration of power in the strongest PDP peaks for both instances, ranging from 75% up to 98%. For the NLoS case, Fig. 7 shows that the power ratio in the strongest MPC varies from $\approx 20\%$ up to 99%. The lowest values are related to the furthest NLoS point in the route where reflection and objects in the street canyon (e.g. parked cars) affect the MPCs. In the nearest NLoS points the power ratio is high because they are closer to the beginning of the street canyon, reducing delay dispersion and concentrating the energy in fewer peaks.

3) Path Loss: Fig. 8 shows the PL values for all the measured points. The path loss values are lower or equal than the Friis free-space propagation model for LoS and higher for the NLoS points with differences up to 17 dB for the furthest point. However, an exception is observed at Tx2-Rx5, which has PL values close to the Friis propagation due to the strong reflections from the walls of the street canyon.

B. Angular power spectrum

Fig. 9 and 10 show the double-directional angular power spectra, again using interpolation to improve the granularity of the plot. The LoS point shows a concentrated power at $\theta_{Tx} = \theta_{Rx} = 0^\circ$ because of the LoS component (see Fig. 9). Additionally, we observe an additional MPC at $\theta_{Rx} = 180^\circ$ due to the back lobe of the antenna. For the NLoS case, Fig. 10 shows a concentrated area with high power due to the street canyon at $\theta_{Tx} = -14^\circ, \theta_{Rx} = -8^\circ$. An additional power concentration is located at $\theta_{Tx} = -12^\circ, \theta_{Rx} = 66^\circ$ where the antenna is facing the opposite wall in the street canyon.

1) Angular spread: Table IV shows the σ° values for both Tx and Rx at all locations. Values are smaller at the Tx than at the Rx, both due to the difference in the scan range, and the elevated nature of the Tx (BS); this behavior is consistent with observations in the literature in lower frequency bands. The difference between Tx and Rx is increased in the NLoS case, because of the absence of the dominant LoS component that tends to keep the angular spread small at both link ends. For $Tx2 - Rx5$, we observed that σ° for Tx and Rx have similar values compared to the LoS cases because its behavior is dominated by the high power MPC coming from $\theta_{Tx} = -6, \theta_{Rx} = -22$.

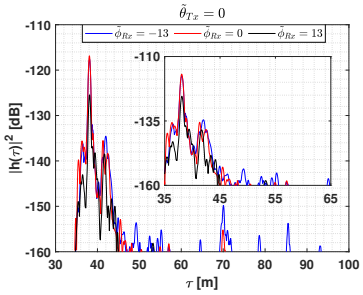

(a) $Tx_2 - Rx_4$, $d = 35\ m$.

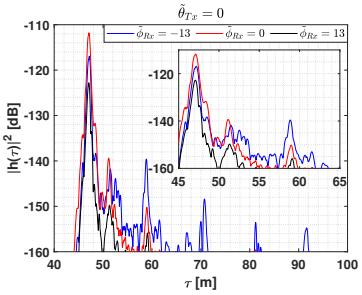

(b) $Tx_2 - Rx_5$, $d = 45.5\ m$.

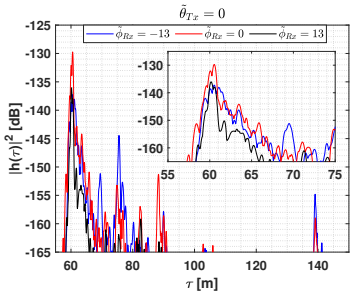

(c) $Tx_2 - Rx_6$, $d = 58.5\ m$.

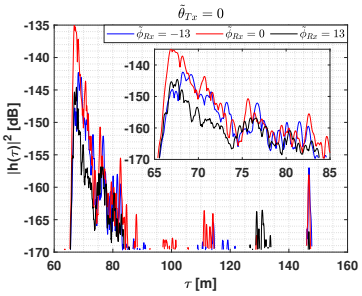

(d) $Tx_2 - Rx_7$, $d = 66.8\ m$.

Fig. 3: Omni-directional NLoS PDPs for different elevations

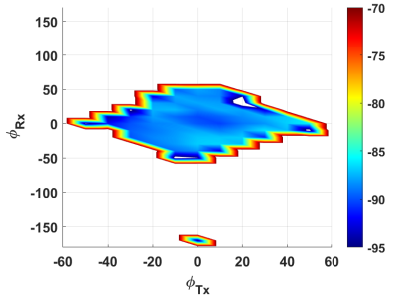

Fig. 4: σ_τ for $Tx_1 - Rx_2$, $d = 57.9\ m$.

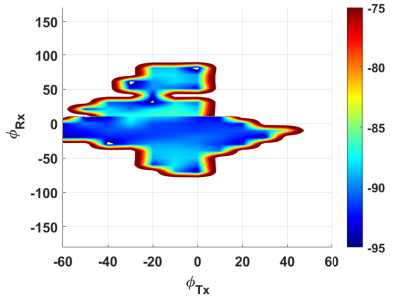

Fig. 5: σ_τ for $Tx_2 - Rx_4$, $d = 35\ m$.

TABLE IV: Angular spread per location.

$AS(\log_{10}(\sigma^\circ))$	Tx	Rx
$\mathbf{Tx_1 - Rx_1}$	0.17	0.24
$\mathbf{Tx_1 - Rx_2}$	0.16	0.24
$\mathbf{Tx_1 - Rx_3}$	0.19	0.25
$\mathbf{Tx_2 - Rx_4}$	0.19	0.35
$\mathbf{Tx_2 - Rx_5}$	0.17	0.2
$\mathbf{Tx_2 - Rx_6}$	0.41	0.45
$\mathbf{Tx_2 - Rx_7}$	0.27	0.51

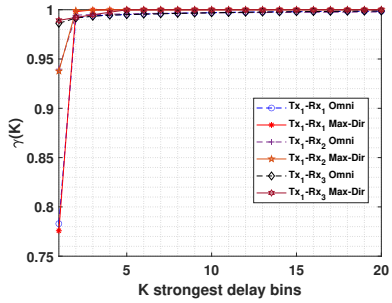

Fig. 6: Power distribution of the K strongest delay bin, LoS case.

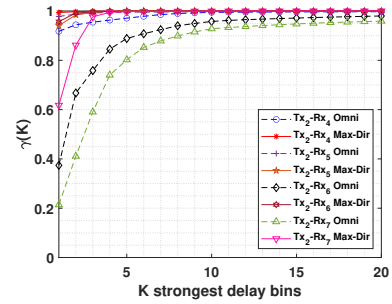

Fig. 7: Power distribution of the K strongest delay bins, NLoS case.

V. Conclusions

In this paper, we presented the results of a double-directional, ultra-wideband (1 GHz bandwidth) measurement campaign performed in a street canyon at a 145 GHz carrier frequency. The campaign was focused on a microcellular

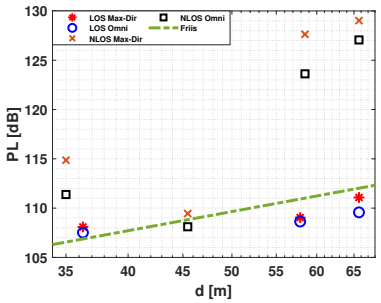

Fig. 8: Path loss comparison.

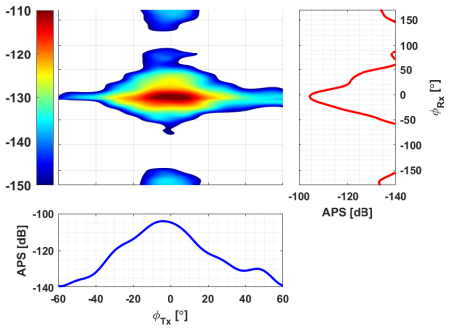

Fig. 9: APS LoS, $Tx_1 - Rx_2$, $d = 57.9\ m$.

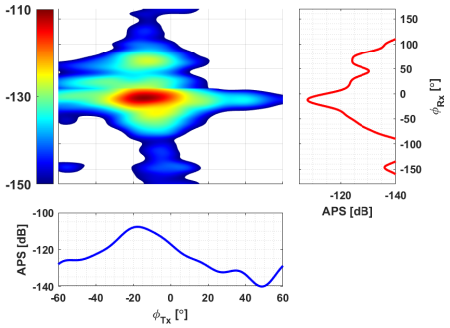

Fig. 10: APS NLoS, $Tx_2 - Rx_4$, $d = 35\ m$.

outdoor urban environment, with distances between 35 to 67 m. The key takeaway from this analysis is that we observe considerable MPCs in the NLoS case, especially for the further distances. We also observe that for NLoS locations near the Tx, reflections of the walls can be strong and occur at levels close to LoS (e.g., Tx2-Rx5). Additionally, for the furthest NLoS points, a rich MPC environment was observed within a 30 dB dynamic range. These insights are useful in the design of high-data-rate communication systems which are very sensitive to nearby interferers. Analyzing the directional behavior of σ_τ allows to determine the dominant paths of the scenarios and how algorithms such as beamforming, power control, or scheduling can manage to supply users within this environment with the required QoS. While the numerical results are specific to the constraints of the current setup's operating parameters, they provide insights into the physics of the propagation and can help the design and development of future THz communication systems and algorithms.

ACKNOWLEDGMENT

This work was partly supported by the Semiconductor Research Corporation (SRC) under the ComSenTer program, NSF under grant number 2133655, NIST under grant number 60NANB21D138, and by Samsung Research America. The work of J. Gomez-Ponce is supported by the Foreign Fulbright Ecuador SENESCYT Program.

REFERENCES

[1] K.-C. Huang and Z. Wang, "Terahertz Terabit Wireless Communication," *Microwave Magazine, IEEE*, vol. 12, no. 4, pp. 108–116, June 2011.

[2] H. Tataria, M. Shafi, A. F. Molisch, M. Dohler, H. Sjöland, and F. Tufvesson, "6g wireless systems: Vision, requirements, challenges, insights, and opportunities," *Proceedings of the IEEE*, vol. 109, no. 7, pp. 1166–1199, 2021.

[3] A. F. Molisch, *Wireless communications*, 2nd ed. IEEE Press - Wiley, 2011.

[4] Y. Xing, T. S. Rappaport, and A. Ghosh, "Millimeter wave and sub-thz indoor radio propagation channel measurements, models, and comparisons in an office environment," *arXiv preprint arXiv:2103.00385*, 2021.

[5] S. Kim and A. G. Zajić, "Statistical Characterization of 300-GHz Propagation on a Desktop," *IEEE Transactions on Vehicular Technology*, vol. 64, no. 8, pp. 3330–3338, Aug 2015.

[6] N. A. Abbasi, A. Hariharan, A. M. Nair, A. S. Almaiman, F. B. Rottenberg, A. E. Willner, and A. F. Molisch, "Double directional channel measurements for thz communications in an urban environment," *arXiv preprint arXiv:1910.01381*, 2019.

[7] N. A. Abbasi, J. Gomez-Ponce, S. M. Shaikbepari, S. Rao, R. Kondaveti, S. Abu-Surra, G. Xu, C. Zhang, and A. F. Molisch, "Ultra-wideband double directional channel measurements for thz communications in urban environments," in *ICC 2021-2021 IEEE International Conference on Communications (ICC)*. IEEE, 2021.

[8] N. A. Abbasi, J. G. Ponce, R. Kondaveti, , S. M. Shaikbepari, S. Rao, S. Abu-Surra, G. Xu, C. Zhang, and A. F. Molisch, "Thz band channel measurements and statistical modeling for urban d2d environments," *arXiv preprint*, 2021.

[9] Y. Xing and T. S. Rappaport, "Propagation measurements and path loss models for sub-thz in urban microcells," *arXiv preprint arXiv:2103.01151*, 2021.

[10] ——, "Millimeter wave and terahertz urban microcell propagation measurements and models," *IEEE Communications Letters*, pp. 1–1, 2021.

[11] N. A. Abbasi, J. G. Ponce, R. Kondaveti, , S. M. Shaikbepari, S. Rao, S. Abu-Surra, G. Xu, C. Zhang, and A. F. Molisch, "Thz band channel measurements and statistical modeling for urban microcells," *to be submitted*, 2021.

[12] N. A. Abbasi, J. Gomez-Ponce, D. Burghal, R. Kondaveti, S. Abu-Surra, G. Xu, C. Zhang, and A. F. Molisch, "Double-directional channel measurements for urban thz communications on a linear route," in *ICC 2021-2021 IEEE International Conference on Communications (ICC)*. IEEE, 2021.

[13] 3GPP, "5G; Study on channel model for frequencies from 0.5 to 100 GHz," 3rd Generation Partnership Project (3GPP), Technical Specification (TS) 38.901, 05 2017, version 14.0.0. [Online]. Available: https://www.etsi.org/deliver/etsi_tr/138900_138999/138901/14.00.00_60/tr_138901v140000p.pdf

[14] J. Gomez-Ponce, D. Burghal, N. A. Abbasi, A. Hariharan, G. Jakhetia, P. Chaganlal, and A. F. Molisch, "Directional delay spread and interference quotient analysis in sub-7ghz wi-fi bands," in *GLOBECOM 2020 - 2020 IEEE Global Communications Conference*, 2020, pp. 1–6.

[15] S. Hur, Y.-J. Cho, J. Lee, N.-G. Kang, J. Park, and H. Benn, "Synchronous channel sounder using horn antenna and indoor measurements on 28 ghz," in *2014 IEEE International Black Sea Conference on Communications and Networking (BlackSeaCom)*, 2014, pp. 83–87.

[16] B. H. Fleury, "First-and second-order characterization of direction dispersion and space selectivity in the radio channel," *IEEE Transactions on Information Theory*, vol. 46, no. 6, pp. 2027–2044, 2000.